ON THE SYNTHESIS OF *N*-SUCCINYLCHITOSAN *BOMBYX MORI* COMPLEXES WITH COBALT(II) IONS AND THEIR INSECTICIDAL PROPERTIES AGAINST *ANACANTHOTERMES TURKESTANICUS* TERMITES

Mamasoliyev Ulugbek Makhammatovich[1,a], Noira Rahimovna Vokhidova[1,b,*], Zuhra Yuldashevna Akhmedova[2,c], Iskandarov Tulkin Iskandarovich[3,d], Sayyora Sharafovna Rashidova[1,e]

[1] – Institute of Chemistry and Physics of Polymers, Scientific Academy of Uzbekistan, Tashkent 100128, A. Kadyri, 7b Str., Uzbekistan
[a] – ORCID: 0009-0006-0906-2592, b – ORCID: 0000-0003-0477-3708,
[e] – ORCID: 0000-0003-1667-4619
[2] – Institute of Zoology, Academy of Sciences of Uzbekistan, Tashkent 100053, Bogishamol 232b Str., Uzbekistan
[c] – ORCID: 0009-0001-6276-1572
[3] – Cabinet of Ministers of the Republic of Uzbekistan, Ministry of Health, Research, Institute of Sanitation, Hygiene and Occupational Diseases, Tashkent 100056, Travel 5th Oltintepa 325 Str., Uzbekistan
[d] – ORCID: 0000-0001-8079-950X
**corresponding author: noira_vokhidova@yahoo.de*

Abstract

*N-succinylchitosan (*N-*SCS) was obtained by the reaction of chitosan derived from Bombyx mori with succinic anhydride mixed at a 1:1 molar ratio in dimethyl sulfoxide for 24 hours at 22°C and pH 7. In order to increase the effectiveness of insecticidal properties,* N-*succinylchitosan complexes with* Co^{2+} *ions (*N-*CSC/*Co^{2+}*) were further obtained. The structural studies show that* Co^{2+} *ions interact with the carboxyl groups of* N-*succinylchitosan. The IR spectra of chitosan,* N-*SCS, and* N-*SCS/*Co^{2+} *show characteristic absorption bands at 1388, 1578, and 473* cm^{-1}*, respectively. Absorption bands characteristic of –NH–CO groups were also noticed at 1674* cm^{-1}*. The concentration dependence of the insecticidal activity of* N-*SCS/*Co^{2+} *solutions was studied, and it was found that a 1.0% solution exhibits 86.7% biological effectiveness against termites. The presented results are helpful for the development of eco-friendly insecticides based on natural polysaccharides.*

Keywords: N-*succinylchitosan, Bombyx mori, cobalt(II) ions, insecticidal properties, termites Anacanthotermes turkestanicus, non-toxic*

Received: 29.01.2025
Accepted: 19.05.2025

1. Introduction

Soluble modification of chitin, chitosan (CS), involves the addition of electron-donating functional groups. These groups can undergo selective reactions within the monomer unit or become ionised. CS is a partially deacetylated chitin derivative that consists of glucosamine, which is structurally similar to glycosaminoglycan and its analogues [1–6]. However, due to the strong intermolecular hydrogen bonding, chitosan is poorly soluble in physiological solvents [7]. This limitation restricts its wide application [8].

N-succinylchitosan (*N*-SCS) is a water-soluble derivative of chitosan. It is synthesised by introducing succinyl groups into the NH_2 group of glucosamine units [9]. The solubility of *N*-SCS in water is helpful in the development of various medical materials, including 3D implants for bone regeneration [10], drug delivery and protein delivery systems [11–13]. *N*-SCS is also scientifically intriguing due to its polyampholyte properties, which allow for control of the ratio of positive and negative charges [14]. Currently, *N*-SCS and polysaccharides such as CS-alginate and CS-hyaluron are cross-linked with multivalent metal ions to form biologically active hydrogels [15].

The interaction of d-metal ions with polysaccharides results in the formation of cross-linked polymer structures, enabling the creation of highly biocompatible hydrogels [16, 17]. Researchers have successfully produced biologically active polymer-metal complexes using CS, *N*-SCS, and polyvalent metal ions such as Au^{3+}, Cr^{2+}, Ba^{2+}, Fe^{3+}, Ca^{2+}, Zn^{2+}, Cu^{2+}, and Pb^{2+} [18–24]. There is a need for the synthesis of new developments that are non-toxic, biocompatible, and biodegradable. These goals can be achieved by modifying the chemical nature of metal ions and controlling the properties of complexes.

To evaluate the biological activity of *N*-SCS, silver nanoparticles (9 - 34 nm in size) were synthesised using *N*-SCS and Ag^+ ions. These nanoparticles exhibited significantly higher antibacterial activity against gram-positive strains (*B. subtilis* ATCC 6633, *B. coagulans* 429) [25]. Similarly, gold nanoparticles (*N*-SCS/Au) were synthesised using *N*-SCS and $HAuCl_4$ salt. These nanoparticles demonstrated high biological efficiency against pathogenic fungi, particularly *Candida albicans* [26, 27]. Furthermore, preparations based on *N*-SCS/Zn/curcumin were studied for their effectiveness against breast cancer cells (MDA-MB-231) as well as two types of bacteria (*Staphylococcus aureus* and *Escherichia coli*) [28]. The authors used *Azadirachta indica*, extracted from Indian Nastarini, as an insecticide in combination with CS. This extract contained neurotoxic compounds commonly used in insect control, such as organophosphates and carbamates. A mixture of Indian mustard extract and CS has proven to be effective against insects [29].

The aim of this study is to obtain a water-soluble *N*-succinylchitosan cobalt (*N*-SCS/Co^{2+}) polymer metal complex by chemically cross-linking *N*-SCS with Co^{2+} ions, and to investigate its physical, chemical, and biological properties.

2. Materials and Methods

2.1. Chemicals

Chitin was isolated from the silkworm *Bombyx mori* cocoon according to the laboratory regulations developed at the Institute of Polymer Chemistry and Physics of the Academy of Sciences of the Republic of Uzbekistan. Chitin isolation and its modification to chitosan were carried out in the following order: extraction of oil, deproteinisation, demineralisation, pigment bleaching, deacetylation of chitin, filtration, washing with water to pH 7, and drying. CS with a molecular mass (MM) of 198 kDa and a degree of deacetylation (DD) of 87% was used in the research. Succinic anhydride was obtained

by dehydration of chemically pure succinic acid. DMSO, NaOH, HCl (chemically pure for analysis), and bidistilled water were also used in the studies.

2.2. Synthesis of *N*-SCS *Bombyx mori*

N-succinylchitosan samples were obtained according to a previously described method [30]. Briefly, a 2% solution of chitosan in acetic acid was titrated with a 5% solution of NaOH until complete polymer precipitation. The precipitate was then washed with bidistilled water until pH 7 was reached and dried in a freeze-dryer at –50°C. In the next stage, a 5% chitosan solution in dimethyl sulfoxide (DMSO) was prepared and filtered. 1 g of succinic anhydride was added. The mixture was stirred for 24 h. Then the resulting reaction mixture of pH 3.5 was titrated with 5% NaOH to pH 5, and the reaction was continued under stirring (800 rpm) for 30 minutes. Next, the resulting dispersion was adjusted to pH 10 - 12 until a light yellow solution of *N*-SCS was formed. The final product was purified from low molecular weight components by dialysis for 72 hours and dried in a freeze dryer.

2.3. Synthesis of *N*-SCS/Co^{2+} Samples

The *N*-succinylchitosan-cobalt (*N*-SCS/Co^{2+}) complex was obtained as follows: 20 ml of a 3% *N*-SCS solution was prepared, filtered and stirred using a magnetic stirrer at 800 rpm for 30 minutes. The *N*-SCS solution of pH 4.19 was titrated with a 0.5 M $CoCl_2$ solution at a rate of 10 μl/s, and the titration was finished when a 1:1 molar ratio was reached. The resulting *N*-SCS/Co^{2+} complex was isolated by precipitation with acetone and dried in a lyophilizer until a constant weight was achieved.

2.4. Methodology

2.4.1. DLS Measurement

Particle size was measured using dynamic light scattering (DLS) (Photokor, Russia). The evaluated sizes ranged from fractions of a nm to 5 - 10 μm. The laser power of the analyser ranged from 2 to 35 mW. The automatic mode of the analyser was used during measurements, processing, and results presentation.

2.4.2. Conductometric Titration

The DD of chitosan was determined by conductometric titration using a Mettler-Toledo AG, Analytical CH-8603 device (Schwerzenbach, Switzerland) [31]. The DD value was calculated using the formula:

$$DD = \frac{C_{NaOH} \cdot (V_2 - V_1) \cdot M}{m} \quad (1)$$

where:

C_{NaOH} – molar concentration of NaOH solution;

V_1, V_2 – the volume of NaOH titrant [ml];

M – the relative molecular mass of a single elementary unit of chitosan [g/mol];

m – the weight of chitosan [g].

2.4.3. UV spectroscopic studies

UV spectroscopic studies were conducted using a SPECORD 210 (Germany) spectrophotometer, with a scanning range of 190 to 1000 nm, a slit width of 1 nm, and a scanning speed of nm per second. The accuracy of UV photometry was determined using potassium dichromate, in accordance with Ph. Eur. guidelines, with an accuracy of ± 0.01.

2.4.4. Elemental Analysis

The nitrogen content in cold samples was determined using the Dumas method. In this method, carbon dioxide is absorbed by an alkali solution, while the nitrogen is collected in a nitrogen meter. The volume of released nitrogen is measured, and its content in the substance is calculated using the formula [32]:

$$N_{total} = \frac{A \cdot V \cdot N}{G} \cdot 100 \quad (2)$$

where:

A – the mass of 1 ml of nitrogen at a given temperature and corrected pressure;
V – the volume of nitrogen [ml];
N – correction factor for a given volume when calibrating a nitrogen meter [m];
G – the weight of sample [mg].

2.4.5. IR-Spectroscopy Analysis

The IR spectroscopic analysis of the starting components and resulting polysaccharides ($CoCl_2$, *N*-SCS, and *N*-SCS/Co^{2+}) was conducted using an IR Tracer-100 (FTIR) spectrometer from BRUKER (Germany). The IR Tracer-100 offers a high signal-to-noise ratio of 60,000:1, a resolution of 0.25 cm^{-1}, and the capability to operate in fast scanning mode, with the ability to register up to 20 spectra per second.

2.4.6. X-ray Diffraction Analysis

X-ray diffraction studies were performed using an XRD-6100 apparatus (Shimadzu, Japan). The diffraction patterns were recorded and controlled by a computer. The XRD-6100 apparatus utilised CuKα radiation with a Ni-filter, operating at a current mode and tube voltage of 30 mA and 30 kV, respectively. The constant detector rotation speed was set at 4°/min with a scanning angle range of 4 to 80°, using a step of 0.02° (ω/2θ coupling).

2.4.7. Atomic Force Microscopy (AFM)

The morphology of the film samples was examined using an AFM Agilent 5500 (USA) microscope at 22°C. Silicon cantilevers with a stiffness of 9.5 N/m and a frequency of 145 kHz were employed. The maximum scanning area in X and Y directions was 15×15 μm^2, while the Z direction was 1 μm. The samples were dried using a lyophilisation ALPHA 1-2 LD plus device at a temperature range from –50 to –55°C and a 0.3 - 0.5 mbar pressure.

2.4.8. Thermal Analysis

Thermal analysis was performed using a synchronous STA PT1600 (LINSEIS, Germany) thermal analyser. The measurements were conducted in an air atmosphere with a heating rate of 10°/min, in a temperature range from 22° to 800°C. The initial mass of the samples was 19.2 mg.

2.4.9. X-ray Fluorescence Method

The content of cobalt(II) ions and ash was determined using the X-ray fluorescence method. A high-performance, energy-dispersive X-ray fluorescence spectrometer (Rigaku NEX CG EDXRF Analyser, set-9022 19 000 0, Rigaku Corporation, Japan) was applied. Before measurement, liquid samples were poured into special cuvettes and covered, while solid or powdered samples were ground and placed into a special cuvette.

The device automatically emits X-rays, reads fluorescent rays, and collects spectral data, displaying the resulting table and graphic spectra at the end of the analysis. The mass fraction (mass, %) with the analytical error (± 0.1 value) is provided for each element.

2.4.10. Study of Insecticidal Properties of Samples

Laboratory tests were conducted at the Institute of Zoology of the Academy of Sciences of the Republic of Uzbekistan. The experiments used termites from the 'Jush ota' region of the Kushrabat district in the Samarkand region. According to the methodology, filter paper, serving as food for the termites, impregnated with the preparation, was placed in sterilised Petri dishes, with 20 working termites placed on each dish. Filter paper soaked in bidistilled water was applied as a control. The dishes were then stored in a dark place, and the number of live, paralysed, and dead termites was assessed. The remaining termites were fed with distilled water for 7 - 10 days. The experiment was repeated five times. The percentage of mortality was calculated using the Abbott formula, taking into account the percentage of mortality in the control group:

$$C = \frac{A\text{-}B}{A} \cdot 100\% \quad (3)$$

where:

C – the biological efficiency [%];
A – the density (number) of the population before exposure;
B – the density (number) of the population after exposure.

3. Results and Discussion

The *N*-SCS/Co^{2+} sample was synthesised based on the procedure described in sections 2.2 and 2.3 according to the scheme in Figure 1.

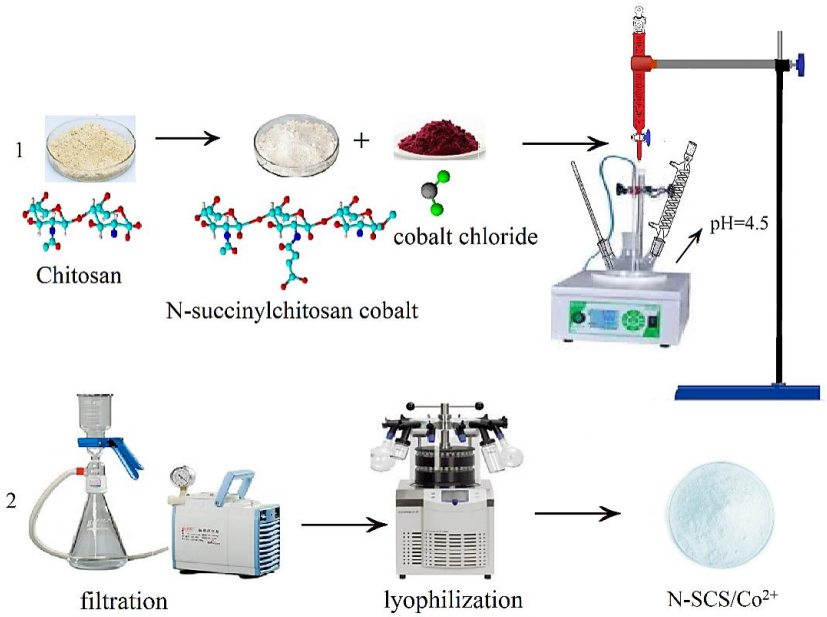

Figure 1. Synthesis sequence of *N*-SCS/Co^{2+} sample departure.

The physicochemical properties of the initial CS and *N*-SCS samples, as well as their *N*-SCS/Co^{2+} derivatives are summarised in Table 1.

Table 1. Some physicochemical characteristics of CS and its derivatives.

Sample	pH	N_{total} [%]	Co^{2+} content [%]	DD [%]	Ash content [%]	η_{rel}
CS	7	8.50	-	87.0	0.89	2.68
N-SCS	7	6.15	-	45.5	0.91	3.30
N-SCS/Co^{2+}	7	5.50	5.83	46.0	6.16	4.41

It was found that the concentration of amino groups in chitosan derivatives decreases, which indicates that the reaction proceeds via $–NH_2$ groups of chitosan. The results of conductometric titration revealed that the N_{total} and $–NH_2$ group percentages in *N*-SCS and *N*-SCS/Co^{2+} were lower by 2.35 - 2.39% and 30 - 41%, respectively, compared to the source chitosan.

The significant increase in ash content in the *N*-SCS/Co^{2+} sample, almost twice that of the original CS and *N*-SCS, can be attributed to the presence of metal ions.

3.1. DLS Analysis

The determination of particle size of CS, $CoCl_2$, *N*-SCS, and *N*-SCS/Co^{2+} in solution was performed using a DLS analyser [33, 34]. The obtained results are presented in Figure 2.

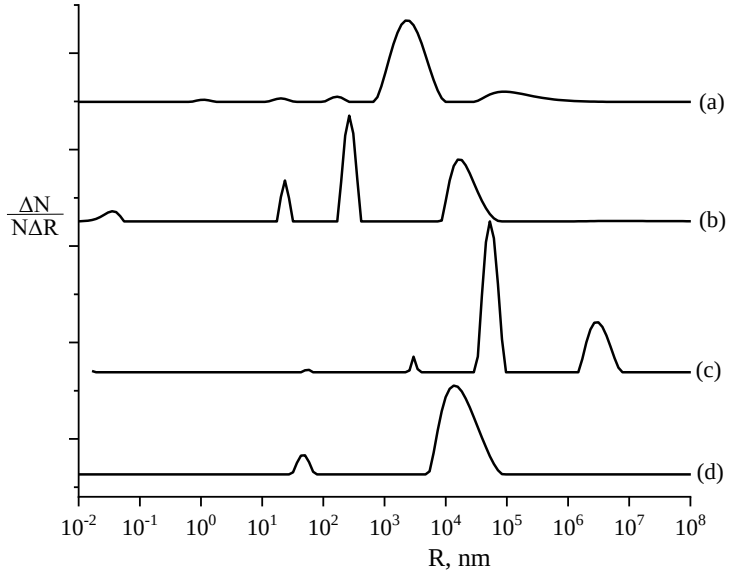

Figure 2. Histogram of particle size distribution of (a) *N*-SCS/Co^{2+}, (b) *N*-SCS, (c) CS, and (d) $CoCl_2$ solutions.

The particle size distribution results indicate that the average hydrodynamic radius of particles in the chitosan solution ranges from 2 to 22 μm. The presence of H–H bonds in the CS macromolecule, its pH-selective solubility, and the chitosan chain's rigidity contribute to the formation of agglomerates in solution. The range is partially reduced to

the nanoscale after modification. 3.1% of *N*-SCS particles exhibit a hydrodynamic radius of 230 nm, while 29% of *N*-SCS particles were observed to be 3.3 μm in size. The hydrodynamic radius of the main fraction of *N*-SCS particles (67.7%) is approximately $5.0 \cdot 10^6$ Å, twice as high as the original CS size. This increase in particle size may be attributed to the degree of polydispersity of the particles due to agglomeration caused by H–H bonds and electrostatic interactions between monomer units.

The particle size in the $CoCl_2$ salt solution is monodisperse, with a hydrodynamic radius of $6.4 \cdot 10^4$ Å. Approximately 93.1% of *N*-SCS/Co^{2+} particles in the solution have a hydrodynamic radius of $2.2 \cdot 10^4$ Å. The Co^{2+} ion may be involved in the formation of *N*-SCS/Co^{2+} by connecting two *N*-SCS molecules through the carboxyl (–COOH) groups via a mutual donor-acceptor bond. Therefore, the hydrodynamic radius of *N*-SCS/Co^{2+} particles is observed to be higher than *N*-SCS.

3.2. UV-Spectroscopy Studies

The results of the UV-spectroscopic studies reveal absorptions in the 216 nm and 238 nm regions for CS (Figure 3). In the *N*-SCS sample, there is a decrease in the absorption intensity at 235 nm and a slight broadening of the absorption region. The reaction of CS with succinic anhydride leads to shifts of the bands in the absorption spectra, indicating the interaction between the amine groups of CS and the carboxyl groups (–COOH) of succinic anhydride, resulting in the formation of covalent bonds.

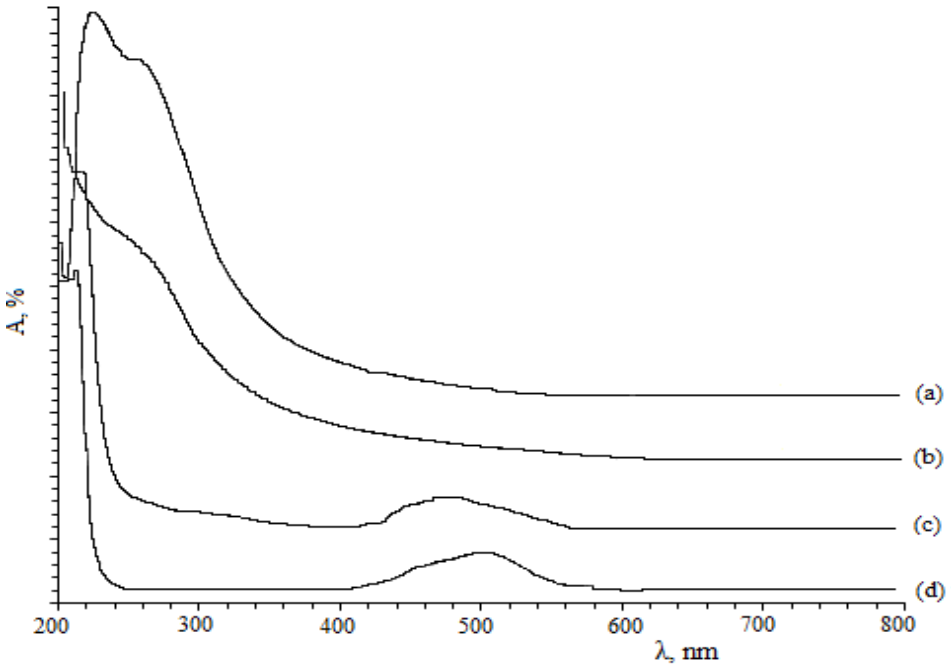

Figure 3. UV spectra of (a) CS, (b) *N*-SCS, (c) *N*-SCS/Co^{2+}, and (d) $CoCl_2$.

In the UV spectrum of solutions containing $CoCl_2$ in *N*-SCS/Co^{2+} salt, broad absorption bands typical of Co^{2+} ions can be observed in the 410 - 550 nm range. The absorption at ca. 480 nm indicates the formation of a donor-acceptor bond between the second carboxyl groups (–COOH) of *N*-SCS and Co^{2+} ions [35].

3.3. IR-Spectroscopy Analysis

IR spectroscopic studies were conducted to observe the structural changes in the initial components after modification (Figure 4). The results show that the IR spectrum of CS exhibited wide absorption valence vibration at 3400 cm^{-1}, corresponding to the vibrations of –OH and $–NH_2$ groups. Moreover, other characteristic bands were also noticed: 1662 cm^{-1} ($\nu_{C=O}$, amide I), 1572 cm^{-1} ($\nu_{C=O}$, $\nu_{C–N}$ and $\delta_{N–H}$, amide II), 3421 cm^{-1} ($\delta_{O–H}$), 1374 cm^{-1} (δ_{CH3}), and 1162 cm^{-1} ($\nu_{C–O–C}$).

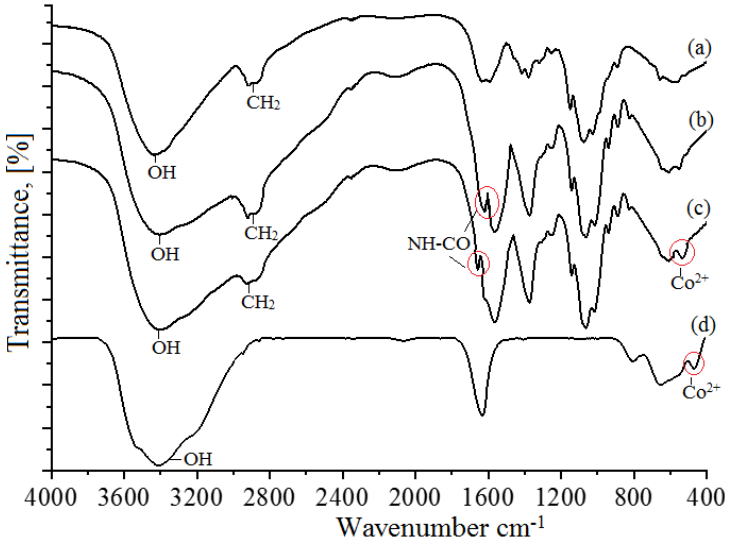

Figure 4. IR spectra of (a) CS, (b) *N*-SCS, (c) *N*-SCS/Co^{2+}, and (d) $CoCl_2$.

When comparing the CS and *N*-SCS spectra, it is observed that the absorption bands at 1557 cm^{-1} ($\nu_{N–H}$, amide II) and 1604 cm^{-1} ($\nu_{C–N}$, amide III) increase in intensity. Additionally, at the 1674 cm^{-1} band, a small shoulder is observed, indicating the chemical reaction between succinate anhydride and the $–NH_2$ groups of chitosan, resulting in the formation of a –NH−CO groups [36, 37]. In the IR spectrum of *N*-SCS/Co^{2+}, the absorption band at 473 cm^{-1} is typical for Co^{2+} ions. It was also observed that the band characteristic of the vibrations of the –NH−CO group became less intense and was shifted to 1694 cm^{-1}. The broad absorption characteristic of –OH groups is clearly visible at 3400 cm^{-1}. Another significant observation is the disappearance of the peak at 1556 cm^{-1} and the increase in the intensity of absorption bands at 1578 cm^{-1} ($\nu_{N–H}$, amide II), indicating the formation of the *N*-SCS/Co^{2+} compound [38–42].

3.4. X-ray Structural Studies

Based on the X-ray diffractograms of *N*-SCS/Co^{2+}, *N*-SCS, CS, and $CoCl_2$ samples (Figure 5), it can be observed that CS exhibits two characteristic peaks. First, a strong peak at 2θ = 20° and second, a weak peak at 2θ = 10° [43, 44]. In the diffractogram of the *N*-SCS sample, the peak at 10° disappears, and there is a decrease in the intensity of the peak at 20°. This decrease in intensity can be attributed to the changes in the CS molecular structure and the formation of an $−NH_2−CO$ bond between the hydroxyl and amino groups [45]. Thus, the obtained results indicate the successful succinylation of CS.

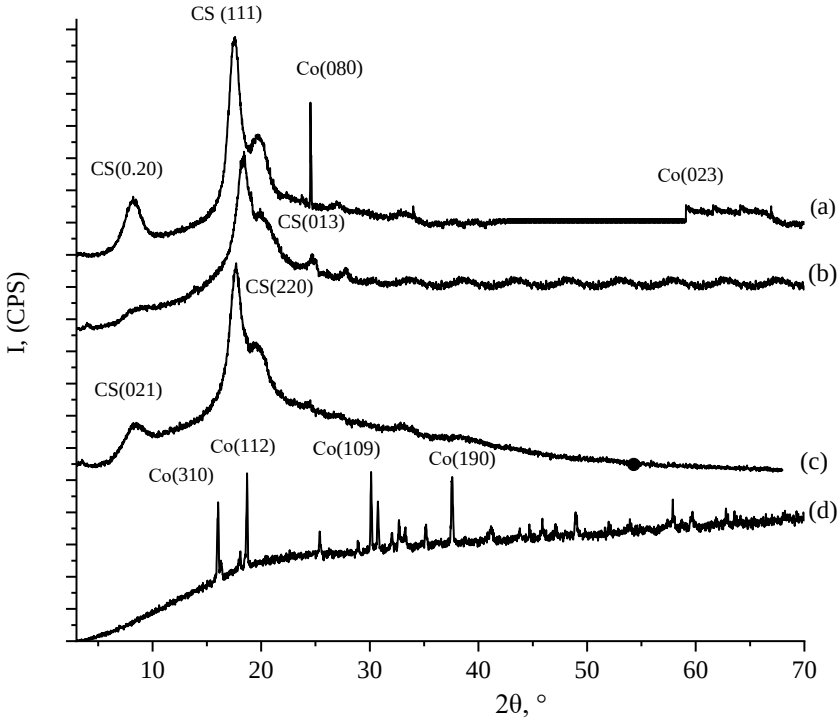

Figure 5. X-ray diffraction patterns of (a) *N*-SCS/Co^{2+}, (b) *N*-SCS, (c) CS, and (d) $CoCl_2$.

In the case of *N*-SCS/Co^{2+}, the intensity of peaks at 2θ = 20° and 2θ = 10° increases. The appearance of a new peak at 2θ = 26° suggests the formation of mutual donor-acceptor bonds between Co^{2+} ions and carboxyl (–COOH) groups of *N*-SCS. As for $CoCl_2$, the diffraction pattern shows peaks at 2θ = 16°, 19°, 31°, 32°, 38°, 50°, and 57°, which correspond to the monoclinic cobalt [46, 47].

3.5. AFM Analysis

The surface of the *N*-SCS and *N*-SCS/Co^{2+} films was analysed using the AFM method [48, 49]. As can be seen in Figures 6 and 7, the morphology of both films revealed an uneven surface, with the presence of spherical and non-spherical particles of various sizes.

The AFM analysis of the *N*-SCS films showed particles ranging in size from 2.98 to 11.9 μm, with an average size of 5.97 μm (Figure 6), while for *N*-SCS/Co^{2+} films, the particle size ranged from 3.28 to 164 μm, with an average size of 5.97 μm (Figure 7).

3.6. Thermal Analysis

Figure 8 shows the DSC thermograms of CS, *N*-SCS and *N*-SCS/Co^{2+} samples. The temperature limits at which thermal and thermooxidative degradation start are essential in evaluation, as they lead to the release of low-molecular compounds.

In the DSC thermogram, the sample moisture loss is represented by an endothermic peak at 98°C. Exothermic peaks at 130 and 254°C in the thermogram of chitosan indicate degradation of this polymer (Figure 8b).

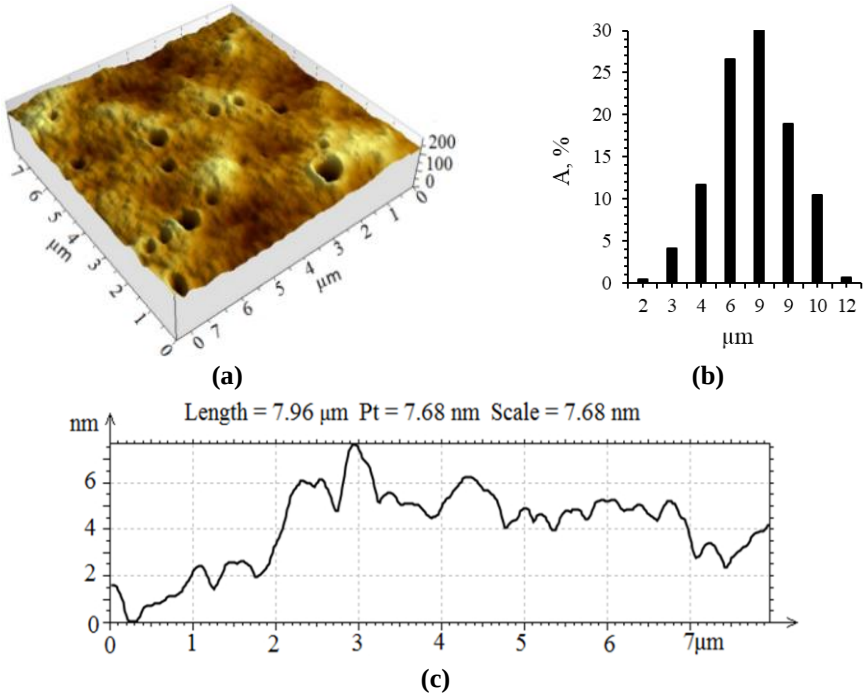

Figure 6. *N*-SCS film (a) AFM image, (b) particle size distribution, and (c) the surface roughness profile.

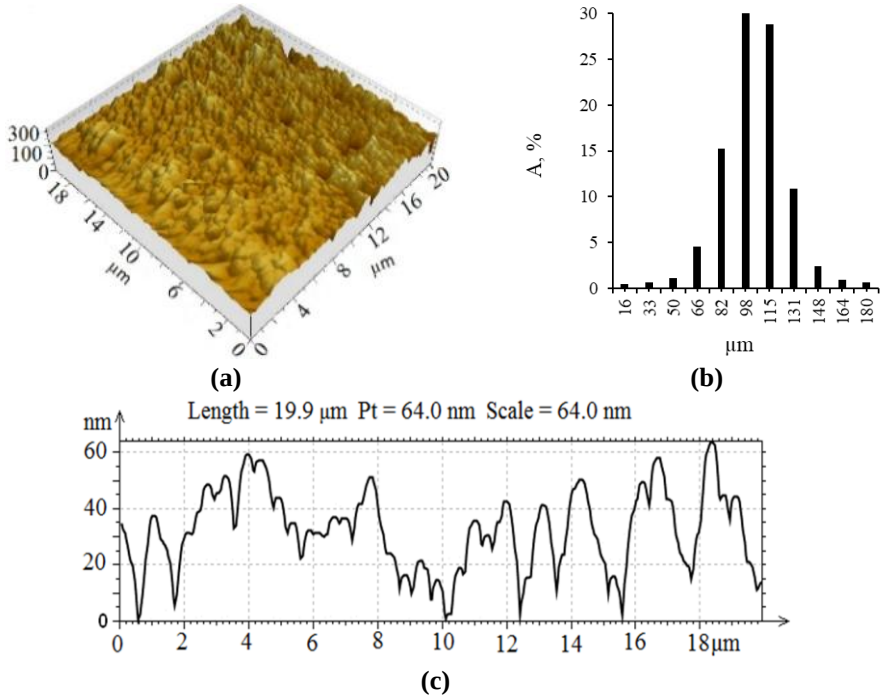

Figure7. *N*-SCS/Co^{2+} film (a) AFM image, (b) particle size distribution, and (c) the surface roughness profile.

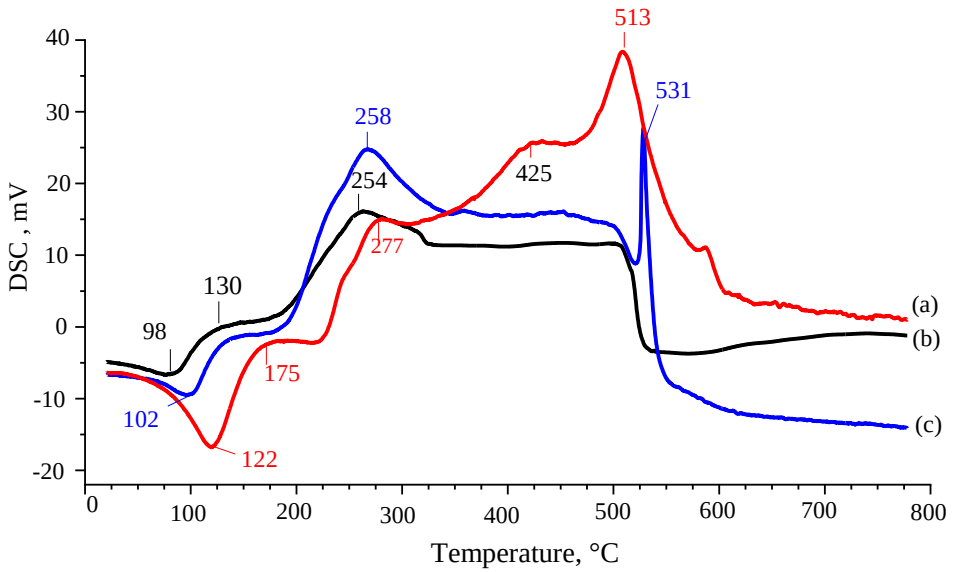

Figure 8. Differential scanning calorimetry thermograms of (a) *N*-SCS/Co^{2+}, (b) CS, and (c) *N*-SCS.

For the *N*-SCS sample, water evaporation occurs at 102°C, while the exothermic peak at 258°C reflects the decomposition of the polymer. Moreover, a new exothermic peak at 531°C was observed, possibly resulting from breaking the covalent bond between the C=O group of succinic anhydride and the $–NH_2$ groups of chitosan.

The water evaporation from the *N*-SCS/Co^{2+} sample is indicated by the endothermic peak at 122°C, while an exothermic peak at 277°C signifies the decomposition of the polymer. The presence of new exothermic peaks at 425 and 513°C can be attributed to the breaking of the covalent bond between the C=O group of succinic anhydride and the $–NH_2$ groups of chitosan, as well as the breaking of the bond between the Co^{2+} ions attached to the second C=O group in succinic anhydride [50].

TG thermogram with derivative DTG curve of CS, *N*-SCS, and *N*-SCS/Co^{2+} polymeric samples (Figures 9 and 10) revealed that weight loss occurred in multiple stages.

In particular, 4.87% mass loss of chitosan in temperatures of up to 201.2°C results from the evaporation of water absorbed and bound to the polymer and solvent desorption (Table 2). At temperatures ranging from 201 to 302°C, 41.7% weight loss, resulting from polymer degradation, is observed. Within higher temperatures, from 302 to 596°C, further mass decrease of 47.15% is noted. This weight loss indicates the dissociation of functional groups, i.e., $–CH_2$ and –CH–OH [51]. The next stage occurs at a temperature range of 596 - 800°C, indicating the evaporation of residual degradation volatile products.

In the TGA and DTA curves of *N*-SCS (Figures 9 and 10), three distinct temperature ranges representing different thermal events and particular weight losses are seen. The first range, up to 222°C (Table 2), shows a 15.89% weight loss resulting from the evaporation of water. Next, the decomposition process takes place between 222°C and 342°C, resulting in a decrease in mass of 39.91%. This process can be attributed to the degradation of $-CH_2$ and −CH−OH groups in CS. The last temperature range, from 343°C to 615°C, shows a further 33.8% mass decrease and is attributed to the decomposition of

the –CH groups, which are formed from the C=O group of succinic anhydride and the $-NH_2$ groups of chitosan [52–54].

The initial weight loss of the *N*-SCS/Co^{2+} sample is caused by the water evaporation, and possibly, the decomposition of low molecular organic substances. This step occurs up to 221°C and refers to Δm of 16.76% (Table 2). The second thermal event occurs from 221 to 281°C. During this stage, oxidation reactions lead to the degradation of $-CH_2$ and −CH−OH groups, causing a weight change of 31.68%. The third thermal event occurs in a 282 - 596°C temperature range, and the 31.93% weight loss is attributed to the fragmentation of the –CH groups and the breaking of the bond between the Co^{2+} ions attached to the $–COO^-$ group in succinic acid [55].

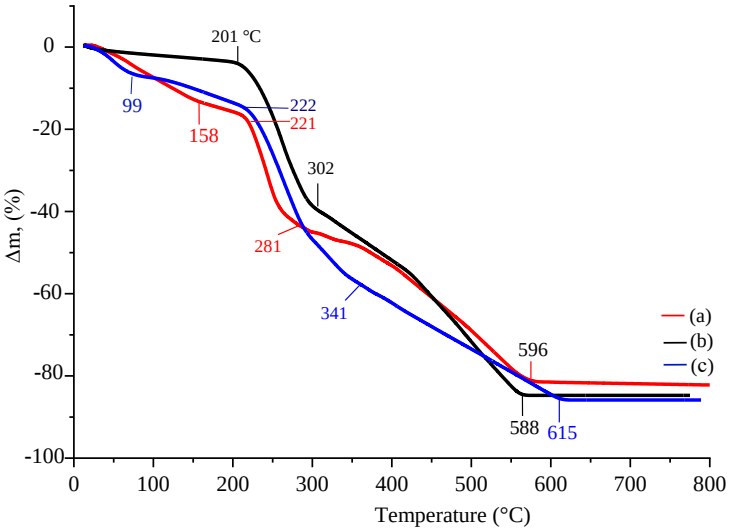

Figure 9. TG thermograms of (a) *N*-SCS/Co^{2+}, (b) CS, and (c) *N*-SCS.

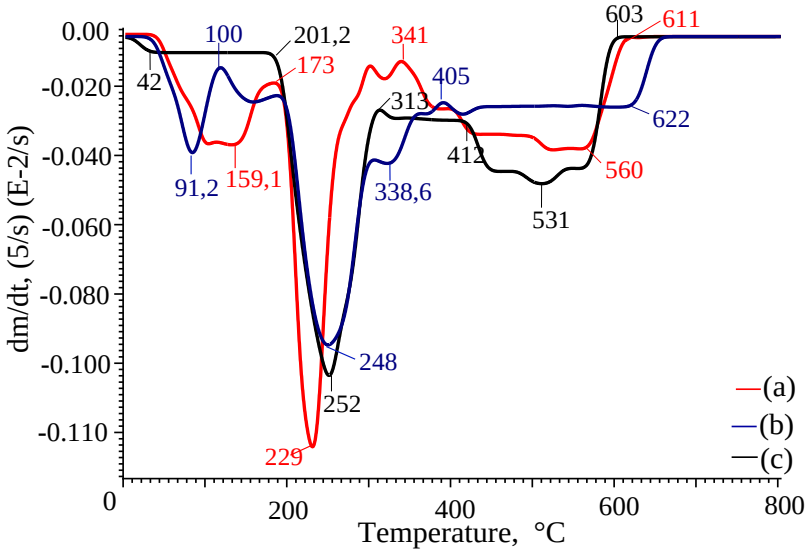

Figure 10. DTG curves of (c) CS, (a) *N*-SCS, and (b) *N*-SCS/Co^{2+}.

Table 2. TG thermal analysis results of CS, *N*-SCS, and *N*-SCS/Co^{2+} samples.

Thermal event	Parameter	Sample		
		CS	***N*-SCS**	***N*-SCS/Co^{2+}**
1st thermal event (low temperature range)	ΔT [°C]	room - 201.2	room - 100	room - 173
	T_{max} [°C]	42	91.2	159.1
	V_{max} [%/min]	0.17	1.81	1.72
	Δm [%]	4.87	15.89	16.76
2nd thermal event (average temperature range)	ΔT [°C]	201.2 - 313	100 - 338.6	173 - 341
	T_{max} [°C]	252	248	252
	V_{max} [%/min]	5.26	5.02	6.43
	Δm [%]	41.07	39.91	31.68
3rd thermal event (high temperature range)	ΔT [°C]	313 - 603	405 - 611	341 - 603
	T_{max} [°C]	531	622	560
	V_{max} [%/min]	2.28	1.08	6.19
	Δm [%]	47.15	33.8	31.93
mass residue [%]		6.91	10.4	19.63

Note. ΔT – temperature range, T_{max} – temperature at maximum rate of weight loss, V_{max} – maximum rate of weight loss at T_{max}, Δm – weight loss

It was also noted that in the second thermal event, the maximum rate of weight loss of the *N*-SCS/Co^{2+} sample is significantly higher (V_{max} = 6.43 %/min) compared to CS (V_{max} = 5.26 %/min) and *N*-SCS (V_{max} = 5.02 %/min). This variation results from the differences in the degradation process. In the case of *N*-SCS/Co^{2+}, it refers to the breaking of the bond between the –CH groups and the Co^{2+} ions attached to the second (–COOH) group in succinic acid, which is observed in *N*-SCS [56, 57].

The overall physicochemical analyses allow us to propose the following mechanism of the *N*-SCS/Co^{2+} synthesis (Figure 11).

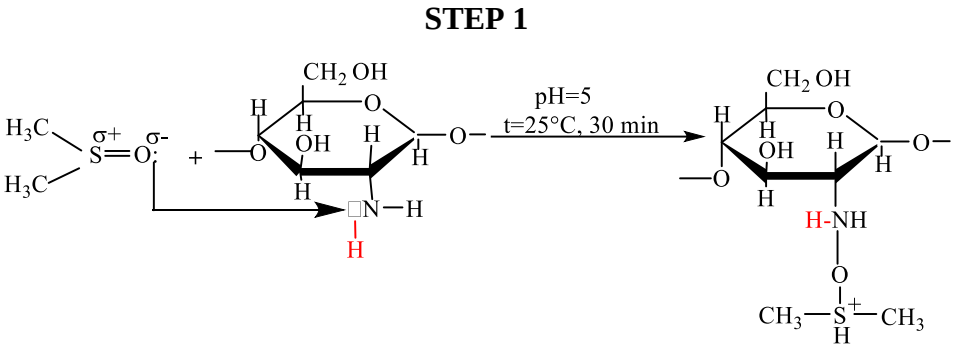

Figure 11. Mechanism of *N*-SCS/Co^{2+} formation.

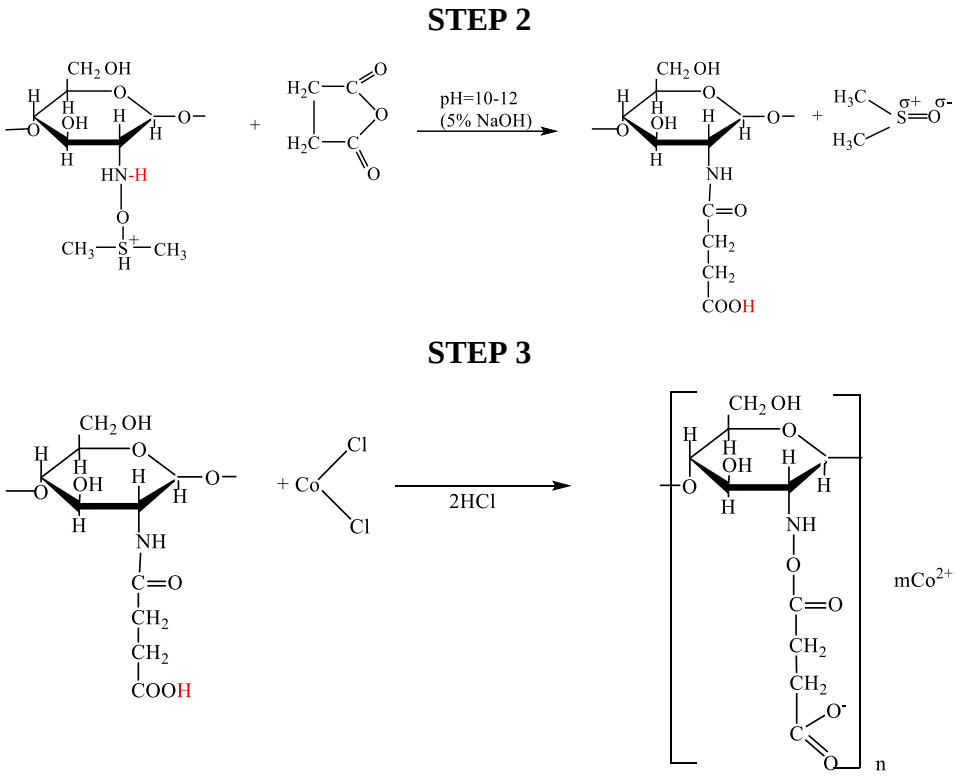

Figure 11. (continued) Mechanism of *N*-SCS/Co^{2+} formation.

3.7. Insecticidal Properties

The insecticidal activity of the *N*-SCS/Co^{2+} was evaluated by testing the samples on termite *Anacanthotermes turkestanicus* larvae. The insecticidal properties were determined by calculating the percentage of mortality using Abbott's formula and comparing it to the mortality in the control group [58–60]. The insecticidal efficiency of the chitosan derivative solution was analysed at different concentrations (Figure 12).

(a) **(b)** **(c)**

Figure 12. The impact of various concentrations of *N*-SCS/Co^{2+} solutions: (a) 0.25%, (b) 0.5%, and (c) 1.0%, on termites.

It was found that on the third day of the experiment, for the trial where termites were fed with filter paper soaked in the 0.25% *N*-SCS/Co^{2+} solution, the mortality rate reached 7.5% (Figure 13a). On the 5th day, the mortality rate increased to 12.5%, and on the seventh day, the mortality rate reached 73.3%. When the concentration was doubled to 0.5% (Figure 13b), the termites' mortality was 11.0%, 57.0%, and 80.0% on the 3rd, 5th, and 7th day. Finally, when termites were exposed to a 1.0% *N*-SCS/Co^{2+} solution (Figure 13c), a mortality of 15.0% was observed on the third day of feeding, followed by 62.5% on the 5th day. On the seventh day, a mortality of 86.7% was recorded, indicating the highest effectiveness of the drug. In contrast, when a 1.0% *N*-SCS solution was taken as a feed, the maximum 74% mortality was found on the seventh day (Figure 13d). The higher efficiency of *N*-SCS/Co^{2+} samples is due to the paralysing effect of Co^{2+} ions on the nervous system and their pheromone properties [61].

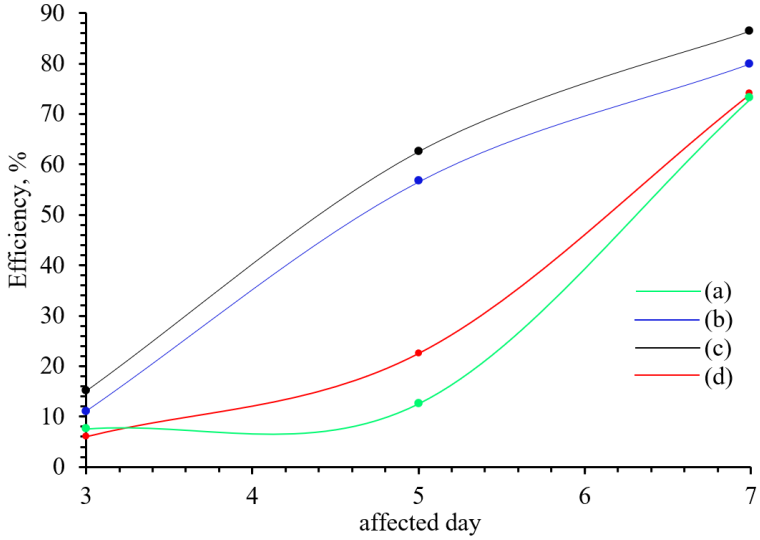

Figure 13. The insecticidal efficiency of *N*-SCS/Co^{2+} solutions of different concentrations, (a) 0.25%, (b) 0.5%, and (d) 1.0%, and of (c) 1.0% *N*-SCS solution.

To confirm the biological properties of the *N*-SCS/Co^{2+} solution, its effect on mulberry silkworm *B. mori* larvae was investigated (Figure 14). Experiments were performed according to the previously developed methodology [62].

The experiment demonstrated that *N*-SCS/Co^{2+} solutions of varying concentrations do not harm beneficial insects. Additionally, mulberry silkworms did not experience any mortality, indicating that the drug is environmentally safe. More specifically, 20 mulberry silkworms, which had completed the first dormancy period, were placed in separate containers and exposed to solutions of *N*-SCS/Co^{2+} of 0.25%, 0.5%, and 1% concentration for 14 days. The silkworms were monitored until they entered the cocooning stage, and no deaths were observed during this period.

The chronic toxicity of the drug was studied using mathematical modelling methods. The threshold and ineffective doses of *N*-SCS/Co^{2+} were established as 30.0 and 6.0 mg/kg, respectively. Moreover, the calculated permissible daily *N*-SCS/Co^{2+} dose (PDD) was 7.2 mg/person/day or 0.12 mg/kg.

(a) **(b)** **(c)**

Figure 14. The effects of different concentrations of *N*-SCS/Co^{2+} solutions on *Bombyx mori* larvae: (a) 0.25%, (b) 0.5% and (c) 1.0%.

In literature, the acute toxicity of the *N*-SCS/Co^{2+} drug was established. Experiments were conducted on white rats. Doses from 5000 to 13000 mg/kg were studied. No animal deaths were noted in any of the experimental groups. It was not possible to calculate the accurate average drug lethal dose, but it was stated that the lethal dose of the drug was > 5000 mg/kg. The drug was thus classified as toxic class IV (low-toxic compounds) [63].

4. Conclusions

To conclude, this study focuses on the synthesis of water-soluble *N*-SCS samples with the addition of cobalt(II) ions. The elemental analysis revealed that the original CS sample is characterised by a higher nitrogen content than the *N*-SCS and *N*-SCS/Co^{2+} samples, with a difference of 2.35% and 2.39%. The presence of Co^{2+} ions was also confirmed in *N*-SCS after modification. The physicochemical properties of the synthesised samples were further investigated. The IR spectrum of *N*-SCS/Co^{2+}showed an absorption peak at 473 cm^{-1}, while the UV spectrum displayed an absorption peak at 480 nm, providing evidence for the *N*-succinylchitosan modification with cobalt(II) ions. Additionally, the *N*-SCS/Co^{2+} diffraction pattern showed the presence of peaks characteristics to the polymer matrix, i.e., at $2\theta = 20°$ and 10°. The new peak at $2\theta = 26°$ can be explained by the formation of a mutual donor-acceptor bond between the carboxyl groups of *N*-SCS and Co^{2+} ions.

When studying the insecticidal properties of *N*-SCS/Co^{2+} solutions at concentrations of 0.25, 0.5, and 1.0%, it was found that the 1% solution exhibited the highest biological effectiveness against termites. *N*-SCS/Co^{2+} compound holds promise as a potential environmentally friendly agrochemical agent for the effective control of termites, which are known to cause significant damage in agriculture.

5. Acknowledgements

This study was conducted with the basic funding of the Academy of Sciences of the Republic of Uzbekistan.

6. References

[1] Bashir S, Teo YY, Ramesh S, Ramesh K, Khan AA; (2015) N-Succinyl chitosan preparation, characterization, properties and biomedical applications: A state of the art review. Rev Chem Eng 31(6), 563–597. **DOI:** 10.1515/revce-2015-0016

[2] Patel MP, Patel RR, Patel JK; (2010) Chitosan mediated targeted drug delivery system: a review. J Pharm Pharm Sci 13(4), 536–557. **DOI:** 10.18433/J3JC7C

[3] Mwakalesi AJ, Umbayda TG; (2024) Chitosan enriched with ZnO nanoparticles fabricated using *Synadenium glaucescens* (Pax) aqueous leaf extract maintains postharvest quality of banana. Appl Food Res 4(2), 100536. **DOI:** 10.1016/j.afres.2024.100536

[4] Bahndral A, Shams R, Choudhary P; (2024) Plant-based chitosan for the development of biodegradable packaging materials. Carbohydr Polym Technol Appl 8(1), 100598. **DOI:** 10.1016/j.carpta.2024.100598

[5] Pan M, Tang ZH, Tu JB, Wang ZC, Chen QH, Xiao RD, Liu HQ; (2018) Porous chitosan microspheres containing zinc ion for enhanced thrombosis and hemostasis. Mater Sci Eng C 85, 27–36. **DOI:** 10.1016/j.msec.2017.12.015

[6] Fahmy H; (2024) Formulation of a developed wound dressing containing chitosan, poly (N-vinyl-2-pyrrolidone), and Carbopol. Egypt J Chem 67(3), 449–455. **DOI:** 10.21608/ejchem.2023.232082.8508

[7] Baldrick P; (2010) The safety of chitosan as a pharmaceutical excipient. Regul Toxicol Pharmacol 56(3), 290–299. **DOI:** 10.1016/j.yrtph.2009.09.015

[8] Tan H, Chu CR, Payne KA, Marra KG; (2009) Injectable *in situ* forming biodegradable chitosan–hyaluronic acid based hydrogels for cartilage tissue engineering. Biomaterials 30(13), 2499–2506. **DOI:** 10.1016/j.biomaterials.2008.12.080

[9] Yamaguchi R, Arai Y, Kaneko T, Itoh T; (1982) Utilization of partially N-succinylated derivatives of chitosan and glycolchitosan as supports for the immobilization of enzymes. Biotechnol Bioeng 24(5), 1081–1091. **DOI:** 10.1002/bit.260240505

[10] Mukhopadhyay P, Sarkar K, Bhattacharya S, Bhattacharyya A, Mishra R, Kundu PP; (2014) pH sensitive N-succinyl chitosan grafted polyacrylamide hydrogel for oral insulin delivery. Carbohydr Polym 112, 627–637. **DOI:** 10.1016/j.carbpol.2014.06.045

[11] Wang Y, Peng W, Liu X, Zhu M, Sun T, Peng Q, Zeng Y, Feng B, Zhi W, Weng J, Wang J; (2014) Study of bilineage differentiation of human-bone-marrow-derived mesenchymal stem cells in oxidized sodium alginate/N-succinyl chitosan hydrogels and synergistic effects of RGD modification and low-intensity pulsed ultrasound. Acta Biomater 10(6), 2518–2528. **DOI:** 10.1016/j.actbio.2013.12.052

[12] Lü S, Liu M, Ni B; (2010) An injectable oxidized carboxymethylcellulose/N-succinyl-chitosan hydrogel system for protein delivery. Chem Eng J 160(2), 779–787. **DOI:** 10.1016/j.cej.2010.03.072

[13] Hyun H, Hashimoto-Hill S, Kim M, Tsifansky MD, Kim CH, Yeo Y; (2017) Succinylated chitosan derivative has local protective effects on intestinal inflammation. ACS Biomater Sci Eng 3(8), 1853–1860. **DOI:** 10.1021/acsbiomaterials.7b00262

[14] Xu P, Bajaj G, Shugg T, Van Alstine WG, Yeo Y; (2010) Zwitterionic chitosan derivatives for pH-sensitive stealth coating. Biomacromolecules 11(9), 2352–2358. **DOI:** 10.1021/bm100481r

[15] Alvarez-Lorenzo C, Blanco-Fernandez B, Puga AM, Concheiro A; (2013) Crosslinked ionic polysaccharides for stimuli-sensitive drug delivery. Adv Drug Deliv Rev 65(9), 1148–1171. **DOI:** 10.1016/j.addr.2013.04.016

[16] Xi M, Tan Y, Qiao Z; (2024) Ternary polymer network hydrogel electrolyte polyvinyl alcohol/polyacrylamide/chitosan toward zinc ion hybrid supercapacitors. J Power Sources 623, 235437. **DOI:** 10.1016/j.jpowsour.2024.235437

[17] Venkatesham M, Ayodhya D, Madhusudhan A, Veera Babu N, Veerabhadram G; (2014) A novel green one-step synthesis of silver nanoparticles using chitosan: catalytic activity and antimicrobial studies. Appl Nanosci 4(1), 113–119. **DOI:** 10.1007/s13204-012-0180-y

[18] Phan TTV, Phan DT, Cao XT, Huynh TC, Oh J; (2021) Roles of chitosan in green synthesis of metal nanoparticles for biomedical applications. Nanomaterials 11(2), 273. **DOI:** 10.3390/nano11020273

[19] Deepthi S, Venkatesan J, Kim SK, Bumgardner JD, Jayakumar R; (2016) An overview of chitin or chitosan/nano ceramic composite scaffolds for bone tissue engineering. Int J Biol Macromol 93, 1338–1353. **DOI:** 10.1016/ j.ijbiomac.2016.03.041

[20] Aleksandrova VA, Futoryanskaya AM, Sadykova VS; (2022) A method of obtaining silver–succinyl chitosan nanocomposites and their antimicrobial activity. Appl Biochem Microbiol 58(5), 641–645. **DOI:** 10.1134/S0003683822050040

[21] Balakrishnan A, Jacob MM, Dayanandan N, Chinthala M, Ponnuchamy M, Vo DVN, Appunni S, Gajendhran AS; (2023) Chitosan/metal organic frameworks for environmental, energy, and bio-medical applications: a review. Mater Adv 4(23), 5920–5947. **DOI:** 10.1039/D3MA00413A

[22] Duan H, Lü S, Qin H, Gao C, Bai X, Wei Y, Wu X, Liu M, Zhang X, Liu Z; (2017) Co-delivery of zinc and 5-aminosalicylic acid from alginate/N-succinyl-chitosan blend microspheres for synergistic therapy of colitis. Int J Pharm 516(1–2), 214–224. **DOI:** 10.1016/j.ijpharm.2016.11.036

[23] Vokhidova NR, Rashidova SSh; (2016) Synthesis and stabilization of cobalt and copper nanoparticles by chitosan *Bombyx mori*. J Inorg Organomet Polym 26(6), 1380–1386. **DOI:** 10.1007/s10904-016-0431-6

[24] Montaser AS, Fouda MMG, Fahmy H; (2024) Fabrication of bio-active wound dressings containing carbopol blends and chitosan. Egypt J Chem 67(10), 319–325. **DOI:** 10.21608/ejchem.2024.268187.9305

[25] Alexandrova VA, Futoryanskaya AM, Sadykova VS; (2020) Silver nanoparticles stabilized with chitosan succinamide: synthesis and antibacterial activity. Appl Biochem Microbiol 56(5), 590–594. **DOI:** 10.1134/S0003683820050026

[26] Dananjaya SHS, Edirisinghe SL, Thao NTT, Kumar RS, Wijerathna HMSM, Mudiyanselage AY, De Zoysa M, Choi D; (2020) Succinyl chitosan gold nanocomposite: preparation, characterization, *in vitro* and *in vivo* anticandidal activity. Int J Biol Macromol 165, 63–70. **DOI:** 10.1016/j.ijbiomac.2020.09.126

[27] Leiva A, Bonardd S, Pino M, Saldías C, Kortaberria G, Radić D; (2015) Improving the performance of chitosan in the synthesis and stabilization of gold nanoparticles. Eur Polym J 68, 419–431. **DOI:** 10.1016/j.eurpolymj.2015.04.032

[28] Ghaffari SB, Sarrafzadeh MH, Salami M, Khorramizadeh MR; (2020) A pH-sensitive delivery system based on N-succinyl chitosan-ZnO nanoparticles for improving antibacterial and anticancer activities of curcumin. Int J Biol Macromol 151, 428–440. **DOI:** 10.1016/j.ijbiomac.2020.02.141

[29] Fahmi MZ, Suwito H, Susilo A, Joeniarti E, Jaswdi AMR, Indrasari N; (2017) Chitosan-based neem seed extract nanocapsules: A new approach on enhancing its effectiveness as an insecticide delivery agent. J Chem Technol Metall 52(6), 1129–1134.

[30] Vokhidova NR, Mamasoliyev UM, Yugay SM, Rashidova SSh; (2023) Synthesis and study of the structure of N-succinyl chitosan *Bombyx mori* and their biological applications. Polym Bull 80(12), 12907–12921. **DOI:** 10.1007/s00289-023-04680-1

[31] Sun S, Wang A, He B, Xiao H; (2006) Adsorption properties of N-succinyl-chitosan and cross-linked N-succinyl-chitosan resin with Pb(II) as template ions. Sep Purif Technol 51(3), 409–415. **DOI:** 10.1016/j.seppur.2006.03.004

[32] Bochek AM, Terekhova EA, Popova EN, Smirnova VE, Yudin VE, Gofman IV, Abalov IV, Lavrent'ev VK; (2022) Aqueous solutions of carboxymethyl chitosan mixtures with methyl cellulose and composite films on their basis. Polym Sci Ser A 64(5), 476–486. **DOI:** 10.1134/S0965545X22700298

[33] Zhang Y, Zhang M; (2004) Cell growth and function on calcium phosphate reinforced chitosan scaffolds. J Mater Sci Mater Med 15(3), 255–260. **DOI:** 10.1023/B:JMSM.0000015485.94665.25

[34] Purohit G, Rawat DS; (2022) Characterization techniques for chitosan and its based nanocomposites. In: Gulati S (ed), Chitosan-Based Nanocomposite Materials. Springer Nature Singapore, Singapore, 79–101. **DOI:** 10.1007/978-981-19-5338-5_3

[35] Ghaffari SB, Sarrafzadeh MH, Fakhroueian Z, Khorramizadeh MR; (2019) Flower-like curcumin-loaded folic acid-conjugated ZnO-MPA-β-cyclodextrin nanostructures enhanced anticancer activity and cellular uptake of curcumin in breast cancer cells. Mater Sci Eng C 103, 109827. **DOI:** 10.1016/j.msec.2019.109827

[36] Rogalsky A, Kwon HJ, Lee-Sullivan P; (2016) The rheological injectability of N-succinyl-chitosan solutions. Carbohydr Polym 151, 1082–1090. **DOI:** 10.1016/j.carbpol.2016.06.029

[37] Gong P, Peng S, He J, Deng M, Jiang B, Wang K; (2011) One-step synthesis of glucose-branched galactomannan. Carbohydr Res 346(13), 1973–1977. **DOI:** 10.1016/j.carres.2011.06.012

[38] Jain N, Rajoriya V, Jain PK, Jain AK; (2014) Lactosaminated-N-succinyl chitosan nanoparticles for hepatocyte-targeted delivery of acyclovir. J Nanopart Res 16(1), 2136. **DOI:** 10.1007/s11051-013-2136-x

[39] Chu X, Yang K, He X, Yu K, Luan Y, He Q, Li Z, Xiang Y, Chen H, Zeng Y, Li YZ, Zhang D; (2024) Cross-linking N-succinyl chitosan-oxidated hyaluronic acid-based hydrogel loaded with bone marrow mesenchymal stem cell-derived exosomes induce bone regeneration in cranial defects. Mater Des 241, 112969. **DOI:** 10.1016/j.matdes.2024.112969

[40] Mukhopadhyay P, Maity S, Chakraborty S, Rudra R, Ghodadara H, Solanki M, Chakraborti AS, Prajapati AK, Kundu PP; (2016) Oral delivery of quercetin to diabetic animals using novel pH responsive carboxypropionylated chitosan/alginate microparticles. RSC Adv 6(77), 73210–73221. **DOI:** 10.1039/C6RA12491G

[41] Bashir S, Teo YY, Naeem S, Ramesh S, Ramesh K; (2017) pH responsive N-succinyl chitosan/poly(acrylamide-co-acrylic acid) hydrogels and *in vitro*

release of 5-fluorouracil. PLoS One 12(7), e0179250. **DOI:** 10.1371/journal.pone.0179250

[42] Elewa BS, Fouad E, Eldougdoug WI, ElDesouky MM; (2024) Synthesis and evaluation of corrosion inhibitor based on copolymeric modified chitosan core-shell nanocomposite. Egypt J Chem 67(6), 137–144. **DOI:** 10.21608/ejchem.2023.238870.8668

[43] Petrova VA, Panevin AA, Zhuravskii SG, Gasilova ER, Vlasova EN, Romanov DP, Poshina DN, Skorik YA; (2018) Preparation of N-succinyl-chitin nanoparticles and their applications in otoneurological pathology. Int J Biol Macromol 120, 1023–1029. **DOI:** 10.1016/j.ijbiomac.2018.08.180

[44] Sultan M, Kassem AF, Moharam ME, Taha G; (2024) Investigation of a novel antimicrobial chitosan packaging hydrogel film based on azoloazine derivative. Egypt J Chem 67(5), 411–426. **DOI:** 10.21608/ejchem.2023.227250.8374

[45] Triunfo M, Guarnieri A, Ianniciello D, Coltelli MB, Salvia R, Scieuzo C, De Bonis A, Falabella P; (2024) A comprehensive characterization of *Hermetia illucens* derived chitosan produced through homogeneous deacetylation. Int J Biol Macromol 271, 132669. **DOI:** 10.1016/j.ijbiomac.2024.132669

[46] Shahabuddin S, Sarih NM, Ismail FH, Shahid MM, Huang NM; (2015) Synthesis of chitosan grafted-polyaniline/Co_3O_4 nanocube nanocomposites and their photocatalytic activity toward methylene blue dye degradation. RSC Adv 5(102), 83857–83867. **DOI:** 10.1039/C5RA11237K

[47] Uvarov V, Popov I; (2013) Metrological characterization of X-ray diffraction methods at different acquisition geometries for determination of crystallite size in nano-scale materials. Mater Charact 85, 111–123. **DOI:** 10.1016/j.matchar.2013.09.002

[48] Bupesh G, Amutha C, Vasanth S, Vijayakumar TS, Pandian K, Balachandar V, Gunasekaran DR; (2017) Enhanced peptide delivery and sustainable release of pleurocidin using N-succinyl chitosan nanoparticle. Nano Biomed Eng 9(4), 324–332. **DOI:** 10.5101/nbe.v9i4.p324-332

[49] Łosiewicz B, Osak P, Kubisztal J; (2023) The effect of a composite chitosan-silver(I) ion coating on the corrosion resistance of the cobalt-chromium-molybdenum alloy in saline solution. Prog Chem Appl Chitin Deriv 28, 75–88. **DOI:** 10.15259/PCACD.28.007

[50] Kajjari PB, Manjeshwar LS, Aminabhavi TM; (2013) Novel blend microspheres of poly(vinyl alcohol) and succinyl chitosan for controlled release of nifedipine. Polym Bull 70(12), 3387–3406. **DOI:** 10.1007/s00289-013-1029-6

[51] Kyzas GZ, Siafaka PI, Pavlidou EG, Chrissafis KJ, Bikiaris DN; (2015) Synthesis and adsorption application of succinyl-grafted chitosan for the simultaneous removal of zinc and cationic dye from binary hazardous mixtures. Chem Eng J 259, 438–448. **DOI:** 10.1016/j.cej.2014.08.019

[52] Ge H, Wang S; (2014) Thermal preparation of chitosan–acrylic acid superabsorbent: optimization, characteristic and water absorbency. Carbohydr Polym 113, 296–303. **DOI:** 10.1016/j.carbpol.2014.06.078

[53] Wang C, Zheng Y, Qiao K, Xie Y, Zhou X; (2015) An environmentally friendly preparation and characterization of waterborne polyurethane hydrogels by polyvinyl alcohol physical cross-linking to improve water absorption. RSC Adv 5(90), 73882–73891. **DOI:** 10.1039/C5RA11109A

[54] Abdel-Monem R, Taha S, El-Sayed AA, Abdelhamid AE; (2024) Enhanced performance of chitosan film containing vinyl imidazole-hydroxyethyl

methacrylate copolymers. Egypt J Chem 67(7), 105–116. **DOI:** 10.21608/ejchem.2023.247947.8851

[55] Ashurov NS, Abdurazakov M, Yugay SM, Atakhanov AA, Gulamjanov KA, Turaev JI, Akhymbetova GD, Rashidova SS; (2022) Structure and thermal properties of chitin and chitosan from various sources. J Phys Conf Ser 2388(1), 012011. **DOI:** 10.1088/1742-6596/2388/1/012011

[56] Gao X, Zhou Y, Ma G, Shi S, Yang D, Lu F, Nie J; (2010) A water-soluble photocrosslinkable chitosan derivative prepared by Michael-addition reaction as a precursor for injectable hydrogel. Carbohydr Polym 79(3), 507–512. **DOI:** 10.1016/j.carbpol.2009.08.033

[57] Huang XY, Bu HT, Jiang GB, Zeng MH; (2011) Cross-linked succinyl chitosan as an adsorbent for the removal of methylene blue from aqueous solution. Int J Biol Macromol 49(4), 643–651. **DOI:** 10.1016/j.ijbiomac.2011.06.023

[58] Qasem Mousavi S, Reza Bandani A, Alaie E; (2020) Combination of antibiotics and chitin synthesis inhibitors for the control of *Microcerotermes diversus* (Isoptera: Termitidae). J Asia Pac Entomol 23(4), 957–962. **DOI:** 10.1016/j.aspen.2020.08.001

[59] Abbott WS; (1925) A method of computing the effectiveness of an insecticide. J Econ Entomol 18(2), 265–267. **DOI:** 10.1093/jee/18.2.265a

[60] Bayen S, Modak D, Roy S, Chakraborti D, Babu A; (2024) Non-chemical management of termite pests: an overview. Int J Trop Insect Sci 44(3), 995–1011. **DOI:** 10.1007/s42690-024-01206-8

[61] Li C, Han Y, Gao T, Zhang J, Xu DX, Wang Y; (2023) Insecticidal activity of metallic nanopesticides synthesized from natural resources: a review. Environ Chem Lett 21(2), 1141–1176. **DOI:** 10.1007/s10311-022-01548-0

[62] Ministry of Agriculture and Water Resources of the Republic of Uzbekistan; (2014) Methodology of complex and accelerated standardization of pesticides in environmental objects. Methodological manual, Tashkent, 130 p. (in Russian)

[63] Scientific Institute of Sanitary of Hygiene and Occupational Diseases; (2015) Hygienic classification of pesticides by toxicity and hazard. Tashkent, 14 p. (in Russian)